

# ELECTRODYNAMICS AT THE HIGHEST ENERGIES

SPENCER R. KLEIN

*Nuclear Science Division, Lawrence Berkeley National Laboratory,  
Berkeley, CA, 94720, USA*

At very high energies, the bremsstrahlung and pair production cross sections exhibit complex behavior due to the material in which the interactions occur. The cross sections in dense media can be dramatically different than for isolated atoms. This writeup discusses these in-medium effects, emphasizing how the cross section has different energy and target density dependencies in different regimes. Data from SLAC experiment E-146 will be presented to confirm the energy and density scaling. Finally, QCD analogs of the electrodynamic effects will be discussed.

## 1 Bremsstrahlung, Pair Production and the Formation Zone

Bremsstrahlung and pair production were described by Bethe and Heitler in 1934.<sup>1</sup> In bremsstrahlung (braking radiation), an electron with energy  $E$  interacts with a target nucleus, and slows down, emitting a photon with energy  $k$  in the process. For interactions with an isolated atom, for  $k \ll E$ , the Bethe and Heitler bremsstrahlung cross section scales as

$$\frac{d\sigma}{dk} \approx \frac{1}{k}. \quad (1)$$

In pair production, a photon fluctuates to an  $e^+e^-$  pair. The newly created electron or positron interacts with the electromagnetic field of a target nucleus, and the pair becomes a real  $e^+e^-$  pair. For photon energies  $k \gg m_e$ , the pair production cross section is independent of  $k$ . Sophisticated calculations of bremsstrahlung and pair production confirm that these energy dependencies hold within a few percent.

Bethe and Heitler treated bremsstrahlung and pair production as occurring at a single point in space. With this assumption, the radiation depends on the change in electron velocity  $\Delta\vec{v}$  due to the scattering from the target, independent of the nature of the force that causes the velocity change. For any interaction, one can determine the expected  $\Delta\vec{v}$  distribution, and, from that, find the bremsstrahlung radiation. With this approach, it is relatively easy to generalize from isolated atoms to a dense medium.

In 1953, Ter-Mikaelian<sup>2</sup> and Landau and Pomeranchuk<sup>3</sup> pointed out that the assumption that the interaction occurs at a single point fails when the incoming particle has a high enough energy. It is impossible to localize the reaction to a point on the projectile's trajectory. This is true classically as well as quantum mechanically. The pathlength over which the reaction can be localized is the formation length,  $l_f$ .

Classically, the formation length is the distance  $z$  over which the phase factor,  $\exp(i[\vec{k}\cdot z - \omega t])$  is roughly constant ( $\vec{k}\cdot z - \omega t < 1$ ). In a vacuum, the photon wave vector  $\vec{k}$  and the photon frequency  $\omega$  are related by  $|\vec{k}|c = \omega$ . The position  $z$  and time are related by the electron velocity.

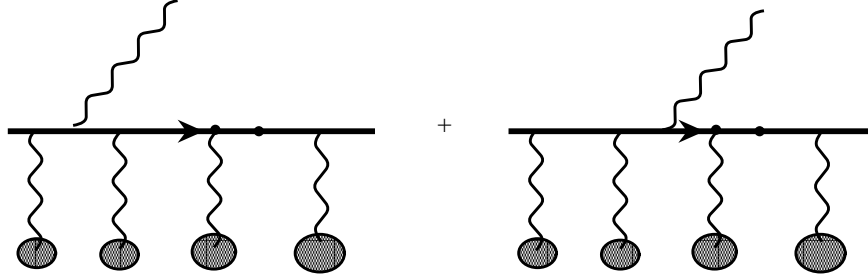


Figure 1: Two Feynman diagrams for bremsstrahlung in a dense medium. If the nuclei are packed densely enough, the amplitudes for these two processes nearly cancel.

The electron moves more slowly than the photon, so eventually the two particles will separate by more than one photon wavelength, at which point they can be considered two separate particles.

Quantum mechanically, the formation length is calculated from the momentum transfer  $q_{||}$  from the target nucleus to the electron-photon system;  $l_f = \hbar/q_{||}$ . The momentum transfer is fixed by the kinematics (4-momentum conservation). For  $E \gg m$  with initial ( $p_e$ ) and final ( $p'_e$ ) electron momenta,

$$q_{||} = p_e - p'_e - k = \sqrt{E^2 - m^2} - \sqrt{(E - k)^2 - m^2} - k \approx \frac{m^2 c^3 k}{E(E - k)} \quad (2)$$

where  $m$  and  $E$  are the electron mass and energy. This holds as long as the photon emission angle  $\theta_\gamma$  is smaller than the typical emission angle  $m/E$ .

Because  $q_{||}$  drops as  $E$  rises,  $l_f$  can be very long for high energy reactions. For example, for a 25 GeV electron emitting a 100 MeV photon,  $l_f = 100 \mu\text{m}$ . For astrophysical energies,  $l_f$  can be hundreds of meters; for  $E = 10^{20}$  eV,  $k = 5 \times 10^{19}$  eV,  $l_f = 160$  m. As (for  $k/E$  fixed)  $E \rightarrow \infty$  and  $l_f \rightarrow \infty$ , interactions with the medium as a whole determine the radiation.

For pair production, the formation length is given in a manner similar to bremsstrahlung.  $l_f = E(E - k)/m^2 c^3 k = 2\hbar k/(M_p^2 c^3)$  where  $M_p$  is the invariant mass of the pair. This formula also applies to photoproduction of quark pairs (vector mesons) in hadronic environments.

The effects of the formation zone have been discussed in several reviews.<sup>4,5</sup>

## 2 Bremsstrahlung Suppression

Landau and Pomeranchuk<sup>3</sup> generalized Bethe and Heitler's concept of radiation from a scattering at a single point, to radiation from the total scattering in a single formation zone. The radiation cannot be localized within the formation zone, so the entire formation zone acts as a single emitter, with radiation determined by the total scattering angle,  $\theta_{MS}$  in this length.

### 2.1 Suppression due to multiple scattering

Bremsstrahlung from relativistic particles is reduced when the scattering angle is larger than  $m/E$ . For an isolated interaction, the usual scattering angle is less than  $m/E$ , so this is relatively unimportant. However, in a dense medium, many scatters add (in quadrature) to a single  $\theta_{MS}$ , and the mean scattering angle can be much larger than  $m/E$ . When this happens, the radiation is reduced. The scattering decreases the electron forward velocity ( $v_z$ ), making the classical phase ( $\vec{k} \cdot z - \omega t$ ) vary more rapidly with  $z$ .

This reduction can also be explained quantum mechanically. Fig. 1 shows the radiation from two pieces of the electron trajectory, separated by a target nucleus. When the nuclei are close enough together (separation much less than  $l_f$ ), the amplitudes for emission from adjacent

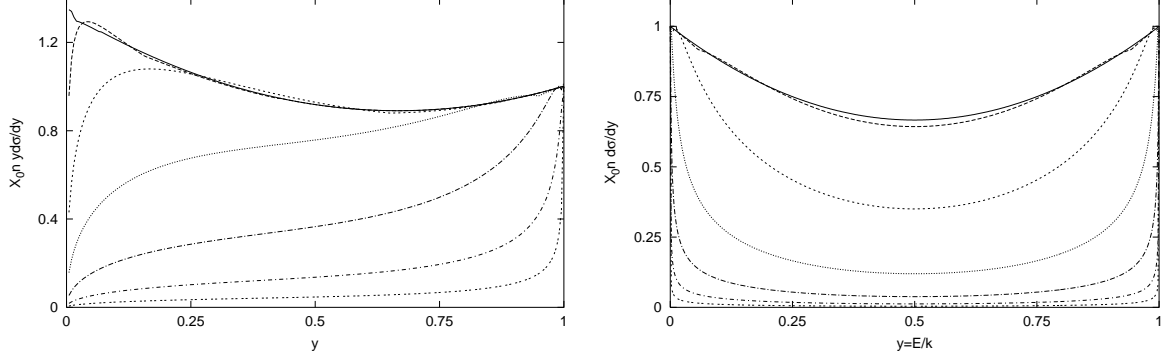


Figure 2: (a) The energy weighted differential cross sections  $y d\sigma/dy$  ( $y = k/E$ ) for bremsstrahlung for electrons with energies  $E = 10$  GeV, 100 GeV, 1 TeV, 10 TeV, 100 TeV, 1 PeV and 10 PeV in lead; as  $E$  increases, the cross section decreases. The units are fractional energy loss per radiation length. (b) The differential cross sections  $y d\sigma/dy$  (Here  $y = E/k$ ) for pair production for photons with energies  $E = 1$  TeV, 10 TeV, 100 TeV, 1 PeV, 10 PeV, 100 PeV and 1 EeV in lead; as the energy increases, the cross section decreases. The units are fractional energy loss per radiation length.

electron lines are almost completely out of phase, and so largely cancel. The target can be thought of as being divided into a small number of independent radiators, each  $l_f$  thick. In a 1956 work, Migdal treated the multiple scattering using the Fokker-Planck equation, and calculated the radiation for each possible path.<sup>6</sup> This approach gave accurate results for the entire  $k/E$  range. However, for pedagogical purposes, this contribution will follow the Landau and Pomeranchuk approach.

Bremsstrahlung is suppressed when  $\theta_{MS} = (E/E_s)^2 l_f / X_0$  is larger than  $m/E$ . Here  $E_s = mc^2 \sqrt{4\pi/\alpha} = 21.2$  MeV,  $X_0$  is the material radiation length, and  $\alpha \approx 1/137$  is the fine structure constant. Defining

$$E_{LPM} = \frac{m^4 c^7 X_0}{\hbar E_s^2} = 7.7 \text{ TeV/cm} \cdot X_0, \quad (3)$$

we find  $\theta_{MS} > m/E$  when  $k/E < (E - k)/E_{LPM}$ . The critical energy,  $E_{LPM}$  ranges from few TeV in solids (4.3 TeV in lead, 2.5 TeV in uranium) up to 540 TeV in water, and 234 PeV in air at sea level. For bremsstrahlung, of course, suppression is present for all  $E$ , as long as  $k/E < E/E_{LPM}$ . This reduction holds for photons emitted at small angles ( $\theta < m/E$ ). Large angle photon emission ( $\theta \gg m/E$ ) already requires a large  $q_{\parallel}$  and is much less suppressed.

In the regime of strong suppression, the bremsstrahlung cross section is

$$\frac{d\sigma}{dk} \approx \frac{1}{\sqrt{k}}; \quad (4)$$

the photon energy dependence changes. The change is due to the reduced coherence. The amplitudes for each bit of path-length  $dz$  in  $l_f$  add in-phase, so the cross section  $\sigma = |\int A(z) dz|^2$ . If a  $z$ -dependent phase reduces the coherence, the cross section is also reduced, even if  $|A|$  is unchanged. A calculation of  $l_f$  including the additional momentum transfer required due to the multiple scattering will yield Eq. (4). Fig. 2(a) shows the cross section following Migdal's calculations. In the limit  $E \gg E_{LPM}$ , suppression is near total except for  $k \approx E$ .

Pair production is suppressed if the produced electron and positron multiple scatter enough. This may be calculated from the bremsstrahlung formulae using the crossing symmetry that relates the two processes. Fig. 2(b) shows the pair production cross sections. Small  $M_p$ , symmetric pairs are suppressed the most; large  $M_p$  asymmetric pairs have a naturally small  $l_f$  and are less subject to suppression. Suppression is significant for  $M_p^2 < km^2/E_{LPM}$ . Of course, since  $M_p \geq 2m$ , suppression requires  $k > 4E_{LPM}$ . When suppression is strong, the pair

production cross section scales as

$$\sigma(k) \approx \frac{1}{\sqrt{k}}; \quad (5)$$

the cross section decreases as  $\sqrt{k}$ , similar to the bremsstrahlung case. For  $k \gg E_{LPM}$ , very asymmetric pairs are created.

## 2.2 Suppression due to photon Compton scattering

Photons from bremsstrahlung are also affected by their environment. The photons can Compton scatter off the electrons in the medium. The collective forward Compton scattering introduces a phase shift in the photons. The shift can be described classically using the dielectric constant of the medium:

$$\epsilon(k) = 1 - \left(\frac{\hbar\omega_p}{k}\right)^2 \quad (6)$$

where  $\omega_p$  is the plasma frequency of the medium;  $\hbar\omega_p$  is typically 40-60 eV for solids. Now,  $|\vec{k}|c = \sqrt{\epsilon}\omega$ , giving the photon an effective mass  $\hbar\omega_p$ . This effective mass ( $\epsilon \neq 1$ ) introduces a phase shift, reducing  $l_f$ . The reduction is significant when  $k < \gamma\hbar\omega_p$ . This inequality is satisfied when  $k/E < \hbar\omega_p/mc^2 \approx 10^{-4}$ . The latter number applies for solids. For smaller  $k$ , the photon mass dominates, and  $l_f = 2ck/\hbar\omega_p^2$  and the cross section scales as<sup>4</sup>

$$\sigma \approx k. \quad (7)$$

The  $k$ -dependence is drastically changed, and the radiation disappears as  $k \rightarrow 0$ . This is sometimes known as the longitudinal density effect or as dielectric suppression. Migdal allowed for dielectric suppression in his calculations, allowing the combined effect to be calculated

As  $k \rightarrow 0$ ,  $q_{\parallel}$  increases and  $l_f$  decreases, actually increasing the localization. Baier and Katkov pointed out that, for sufficiently small  $k/E$ , the interaction may be localized to within the atomic nucleus, and the nuclear form factor affects the emission.<sup>7</sup>

Because of this suppression, the infrared divergence completely disappears! The medium eliminates the need for artificial cutoffs. The total bremsstrahlung cross section is then finite. For example, a 25 GeV electron in lead emits about 10 photons per radiation length.

## 2.3 Mutual Suppression of Bremsstrahlung and Pair Production

At sufficiently high energies,  $l_f > X_0$ . Then, a nascent photon from a bremsstrahlung interaction will convert to an  $e^+e^-$  pair before it is fully formed. The pair production is localized (to within its own  $l_f$ ), and can be used to better locate the bremsstrahlung. This localization reduces the formation length. In the simplest approach one can limit the formation length to  $X_0$ .<sup>8</sup> Then  $\sigma/\sigma_{BH} = X_0/l_f$  and

$$\frac{d\sigma}{dk} = k^0 \quad (8)$$

*i.e.*  $d\sigma/dk$  is independent of  $k$ . After accounting for LPM and dielectric suppression, this effect appears for  $E > E_p = X_0\omega_p E_s/\sqrt{2}c$ , with  $E_p$  about 24 TeV in lead, rising to 205 TeV in aluminum, 540 TeV in water and 15 PeV in sea level air. It appears for intermediate energy photons, as is shown in Fig. 3.

A similar effect occurs for pair production. One of the produced leptons will emit a bremsstrahlung photon, thereby localizing the pair production and reducing  $l_f$ .

A more sophisticated calculation would treat the bremsstrahlung and pair production as a single Feynman diagram, finding the amplitude for the combined interaction. As the incident energy rises, the amplitudes for more and more generations of the electromagnetic shower become intertwined, and the calculation become intractable.

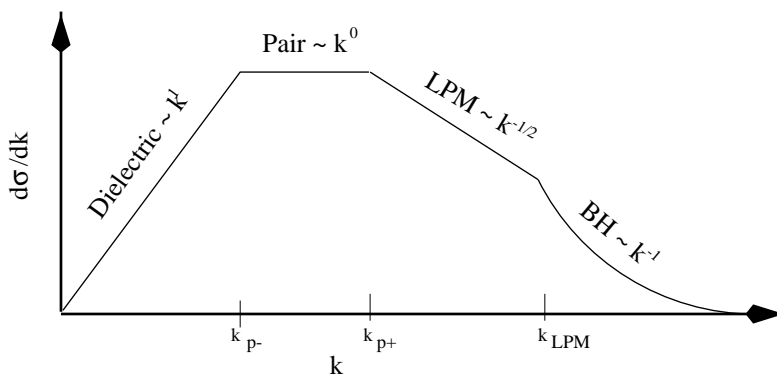


Figure 3: Schematic view of bremsstrahlung  $d\sigma/dk$  with several suppression mechanisms, showing the different  $k$  ranges. For  $E < E_p$ , the pair creation suppression disappears and LPM suppression connects with dielectric suppression.

#### 2.4 Finite Targets and Surface Radiation

The calculations discussed so far only apply to infinite targets. Finite thickness targets have surfaces which can affect the radiation. The simplest case is a very thin target, with thickness  $T$  less than  $l_f$ . Then, the target interacts as a whole, and the radiation depends on the total scattering in the target:<sup>9</sup>

$$\frac{dN}{dk} \approx \ln\left(\frac{1720T}{X_0}\right) - 1. \quad (9)$$

Here,  $dN/dk$  is the radiation from the entire target. The radiation depends only logarithmically on the target thickness! It is important to accurately model for the Coulomb scattering. The usual Gaussian approximation underestimates the number of large angle scatters, and hence the radiation. Eq. (9) is based on an accurate distribution. The radiation will vary from electron to electron, depending on the scattering. Electrons that scatter a lot will emit more radiation than those that scatter less.

For thicker targets, it is conceptually simple to consider the radiation as coming from a bulk target plus the entrance and exit surfaces. This surface radiation is naturally treated as a type of transition radiation. As long as absolute rigor is not required, this is a fruitful approach.

Conventional transition radiation is due to the adjustment that an electrons electromagnetic fields make when they enter a medium with a different dielectric constant. The fields must make a comparable adjustment when the electron enters a medium with a different amount of multiple scattering per unit length; the multiple scattering causes the electron to jitter and the electron drags the fields with it. Ter-Mikaelian pointed out that both types of transition radiation depend on the difference in formation length between the two media:<sup>4</sup>

$$\frac{dN}{dk} \approx (l_f - l'_f)^2. \quad (10)$$

In the 1960's, several calculations of this transition radiation appeared. Although the basic methods were similar, the numerical results were not.

Newer calculations have treated the target as an integrated whole, with good results. These calculations incorporated many advances; a fuller description and references is given in Ref. 5. Almost all of the calculations allowed for electrons traversing arbitrary density profiles. The path is considered as a whole, including interference between radiation from each pair of points on the trajectory. Most of the calculations used accurate models of the Coulomb potential instead of the Gaussian scattering model. Both elastic and inelastic (electron-electron) scattering were included.

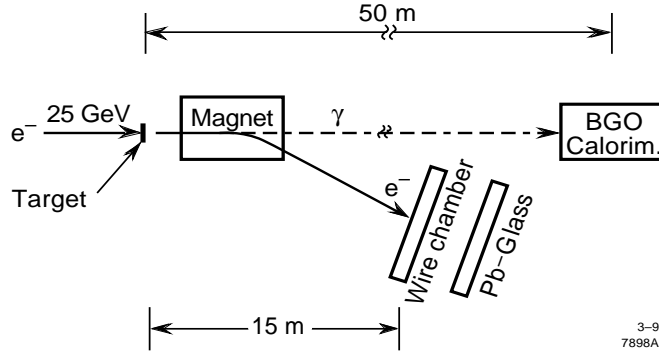


Figure 4: A block diagram of SLAC Experiment E-146 in End Station A. Electrons traversed a thin target and were bent downward into a set of wire chambers and lead glass blocks. Bremsstrahlung photons travelled 50 m downstream into a BGO calorimeter.

## 2.5 Experimental Tests

Shortly after Migdals work appeared, several groups tried to measure LPM suppression of pair conversion from very high-energy photons in cosmic rays. These early experiments all suffered from very limited statistics, typically 1-50 events. The first accelerator experiment, at Protvino in 1976, used 40 GeV electrons interacting in solid targets.<sup>10</sup> Their data indicated that there was some suppression. Later, Kasahara studied the development of  $\approx 100$  TeV showers in lead/emulsion chambers, and found a significant elongation, matching the LPM predictions.<sup>11</sup> This study is of special interest because it is the only experiment to probe the region  $E \approx E_{LPM}$ .

The first accurate measurement was by SLAC experiment E-146,<sup>12,13</sup> in 1993. The collaboration studied bremsstrahlung of 200 keV to 500 MeV photons from 8 and 25 GeV electrons in 7 different target materials. At least two different thicknesses were used for each target material. The target thicknesses were optimized to trade off between multiple interactions in thick targets vs. transition radiation in thin targets. As Fig. 4 shows, electrons interacted in a thin target and were magnetically bent downward into a set of momentum-measuring wire chambers and electron-counting lead glass blocks. A 45 crystal array (7 by 7, minus the 4 corners), 18  $X_0$  thick BGO calorimeter detected the emitted photons. The calorimeter segmentation was used to determine the photon position.

The collaboration took great care to minimize systematic errors. The experiment took data at 120 Hz, and only bunches containing a single electron were used for the analysis. The electron beamline upstream of the target was kept in vacuum to minimize bremsstrahlung from air. The calorimeter was calibrated by two independent methods.

Semi-independent analyses were performed for  $k > 5$  MeV and  $k < 5$  MeV photons. For  $k > 5$  MeV, most photon interactions in the calorimeter were pair conversions. At lower energies, Compton scattering dominated. Also, for the 25 GeV beams, synchrotron radiation from the bending magnets was significant for  $k < 1$  MeV. Most of this radiation was from the downward bend by the spectrometer magnet, with a much smaller contribution from the beam-line steering magnets (not shown). The contribution from the spectrometer magnet was largely removed by dividing the calorimeter into diagonal quadrants. Data from the bottom quadrant, where most of the synchrotron radiation hit, was not used. For  $k > 5$  MeV, the systematic error was 5%. Below 5 MeV, the systematic error was 9% for the 8 GeV electrons, rising to 15% for the 25 GeV electrons. The increase is because of the synchrotron radiation removal cut, because the cut efficiency depends on how well the beam is centered.

Some of the E-146 cross section ( $d\sigma/dk$ ) data is shown in Figs. 5 -7. The histogram bin widths are proportional to  $\ln(k)$ . With logarithmic bins, the Bethe-Heitler  $d\sigma/dk \approx 1/k$

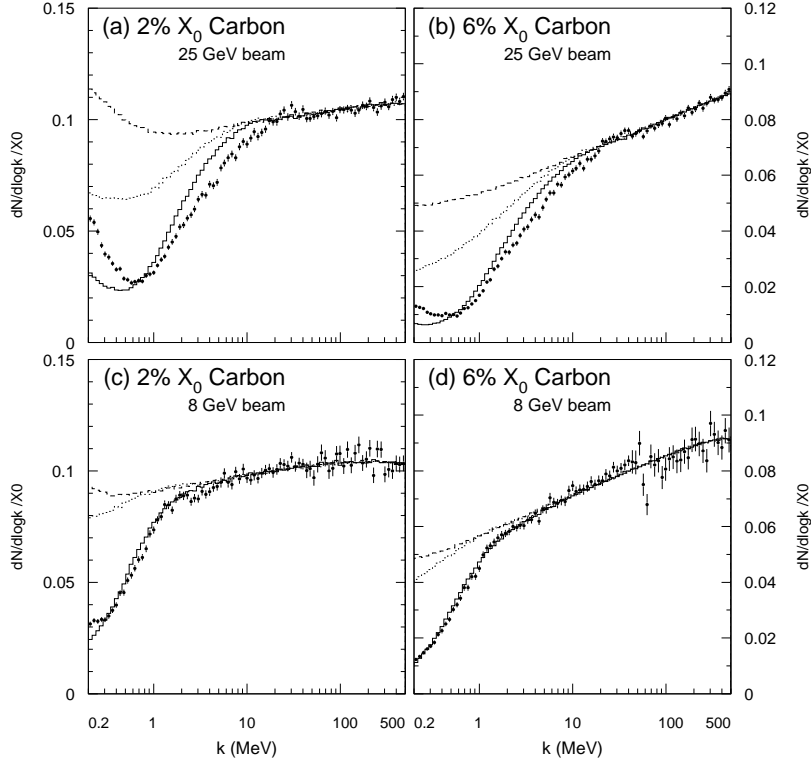


Figure 5: SLAC-E-146 data for 200 keV to 500 MeV photons from 8 and 25 GeV electrons passing through carbon targets. The cross sections are given as  $dN/d(\ln k)/X_0$  where  $N$  is the number of events per photon energy bin per incident electron, for (a) 2%  $X_0$  carbon and (b) 6%  $X_0$  carbon targets in 25 GeV electron beams, while (c) shows the 2%  $X_0$  carbon and (d) the 6%  $X_0$  carbon target in an 8 GeV beam. Three simulations are shown. The solid histogram shows LPM and dielectric suppression of bremsstrahlung, plus conventional transition radiation. Also shown are the Bethe-Heitler plus transition radiation (dashed histogram) and LPM suppression only plus transition radiation (dotted histogram) simulations.

becomes  $d\sigma/d\ln(k)$  which does not vary with  $k$ . The Bethe-Heitler simulations (dashed lines) in Fig. 5 are sloped because a single electron traversing a target may interact more than once; the multiple interaction probability increases with the square of the target thickness. Figure 5 shows 3 simulations: one based on the Bethe-Heitler cross section, one with LPM suppression alone, and the last with LPM and dielectric suppression. Both mechanisms are required to explain the data. For the 25 GeV electrons, the upturn in the simulations for  $k < 500$  keV is due to conventional transition radiation. The data has a similar, but larger upturn. This may be due to some remaining synchrotron radiation from the electron bending magnets.

For the 25 GeV carbon data, the simulation and the data are not in complete agreement for  $k < 15$  MeV. This discrepancy is puzzling. The amorphous graphite target had a micro-crystalline structure, with non-uniform density at a length scale comparable to  $l_f$ . However, if this were a problem, it should also have appeared in the 8 GeV data.

For heavier targets, the suppression is much larger and the agreement is better. For example, Fig. 6 compares the E-146 uranium target data with an LPM plus dielectric suppression simulation (solid line). For  $k > 5$  MeV, the agreement is excellent for both targets at both 8 and 25 GeV. At lower energies, the data is above the simulations. The difference could be due to the additional transition radiation discussed earlier. The other curves in the figure show different predictions of transition radiation; none fit the data. The other targets are believed to be homogenous, with the possible exception of thin oxide layers on the surfaces.

The collaboration also studied thin targets. Figure 7 shows the data for a 0.7%  $X_0$  ( $3.2\mu\text{m}$ )

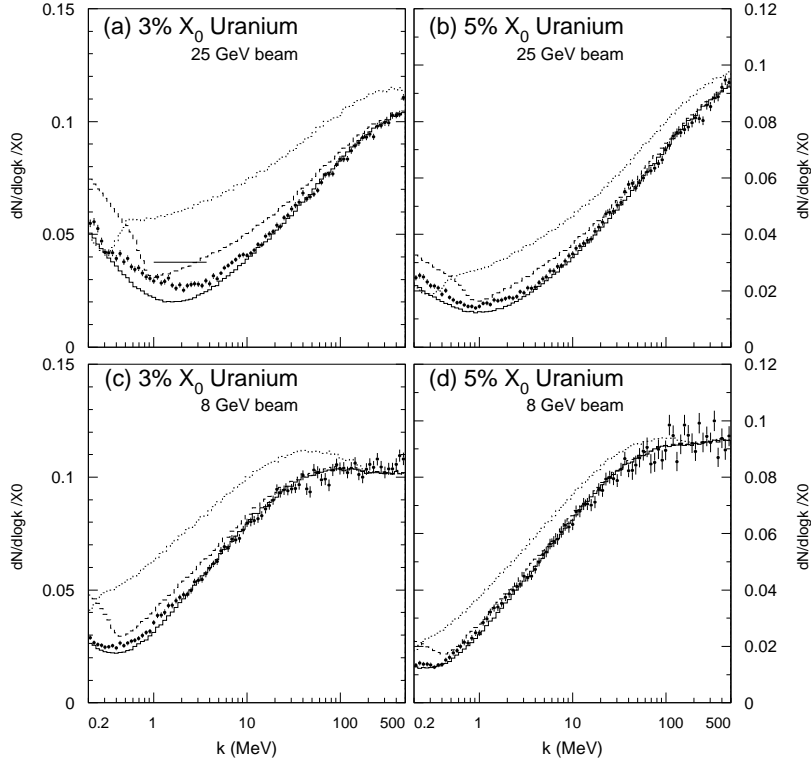


Figure 6: SLAC E-146 measurements and simulations for 3%  $X_0$  and 5%  $X_0$  uranium targets in 8 and 25 GeV electron beams. The solid histogram shows a simulation with LPM and dielectric suppression and conventional transition radiation. The other simulations use different calculations of transition radiation due to multiple scattering.<sup>12</sup> The solid line in panel (a) is based on Eq. (9).

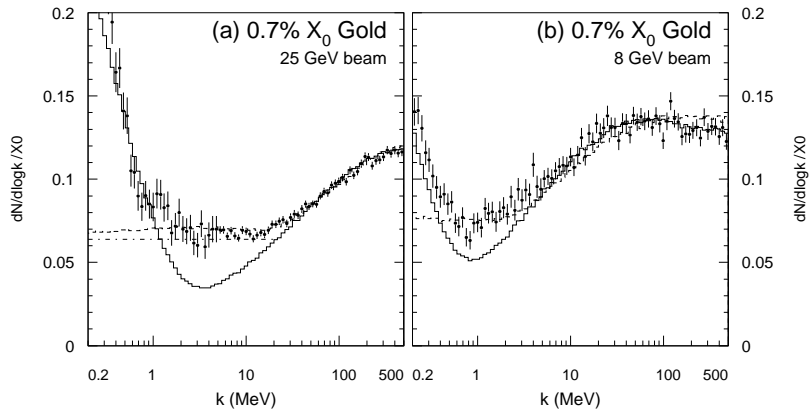


Figure 7: SLAC E-146 data on 8 and 25 GeV electrons hitting a 0.7%  $X_0$  gold target. Shown are calculations by Blankenbecler and Drell (dashed line), and using Eq. (9) (dot-dashed line). The solid histogram is a simulation assuming Migdal plus dielectric suppression.



thick gold target. For 25 GeV electrons in this target,  $l_f > T$  for  $1 \text{ MeV} < k < 7 \text{ MeV}$ . In this range the data is considerably above the LPM plus dielectric prediction. However, calculations using the thin-target limit, Eq. (9), or based on whole-target approaches work well; the dot-dashed line in the figure is based on Eq. (9) while the dashed line is a whole-target calculation by Blankenbecler and Drell.

In short, for  $E \ll E_{LPM}$ , the LPM effect seems to be understood to the 10% level in a variety of regimes. For higher energies, the effect is clearly there, but good measurements are needed to confirm the formulae.

### 3 QCD Analogs

The problem of hadrons traversing a hadronic medium is closely related to that of electrons traversing a charged medium. Reactions involving small momentum transfer are poorly localized, and the overall environment must be considered.<sup>15</sup> This is true at both the hadronic and partonic level. Here, we will consider two very diverse examples: a quark or gluon traversing a nuclear environment, and vector meson photoproduction in a nucleus.

Vector meson photoproduction is a fairly well studied process, with many similarities with  $e^+e^-$  pair conversion.<sup>14</sup> A photon fluctuates to a virtual  $q\bar{q}$  pair. The  $q$  or  $\bar{q}$  interacts elastically with the target nucleus, and the pair emerges as a real vector meson. The elastic scattering can be modelled by Pomeron exchange. The details are unimportant here; our interest is in the target atomic number ( $A$ ) dependence. The nuclear radius  $R_A \approx 1.2A^{1/3} \text{ fm}$  and  $l_f = 2\hbar k/M_V^2$ , where  $M_V$  is the vector meson mass. For  $\rho$  production in lead,  $l_f > R_A$  for  $k > 20 \text{ GeV}$ , and the nucleus interacts as a whole. In this regime, one can further differentiate two regimes. For vector mesons where the  $q\bar{q}$  scattering cross section is small ( $J/\psi$  or  $\Upsilon$ ), the pair will likely undergo a single interaction in the nucleus. Then, the interaction amplitudes from the different nucleons add coherently, and  $\sigma \approx A^2$ . If the  $q\bar{q}$  dipole is large (the  $\rho$ ), then a single pair can interact with many nucleons. As with the LPM effect, the interference is destructive, and the effects of the interior nucleons disappear. In effect, the  $q\bar{q}$  pair sees only the front surface of the nucleus, with area  $A^{2/3}$ , and  $\sigma \approx A^{4/3}$ . At lower  $k$ , where  $l_f \ll R_A$ , the interactions are independent, and  $\sigma \approx A$ . So, simple kinematics considerations lead to 3 different  $A$ -scaling regimes, independent of the details of the interaction.

In contrast, quark or gluon (parton) energy loss in dense media is still not well understood. A parton produced in a relativistic heavy ion collision will interact and lose energy to the surrounding medium, be it hot nuclear matter or a quark gluon plasma.<sup>16</sup> For most of the energy-loss interactions,  $l_f > R_A$  and interference between multiple interactions is important. The previously discussed 'thin target' approach applies: the energy loss should be calculate based on the total scattering angle.

The created partons are bare, without an accompanying colored fields. Because of the retarded potentials, newly created partons (or electrons) will take some time to grow accompanying colored (or electromagnetic) fields. Until these fields are fully formed, the interaction cross sections will be reduced. Because of these effects, the total energy loss grows as  $L^2$ , where  $L$  is the distance traversed in the medium.

One key question concerns where the lost energy goes. Experiments reconstruct jets by measuring energy deposited in a cone. If the energy lost by the parton is transferred to soft particles which remain in the jet cone, the measured jet energy will be unaffected. The energy loss can only be measured by studying the energy of the individual particles in the jet. However, if the soft particles scatter outside the jet cone, the measured jet energy will be unchanged. Bremsstrahlung suppression is angular; photons emitted with angles  $\theta_\gamma \gg m/E$  are much less suppressed. So, in the strong suppression limit,  $\theta_\gamma \gg m/E$ . Because the angular dependence is entirely due to kinematics, the same effect should apply in QCD. When suppression is strong,

radiated gluons are more likely to be outside the jet cone.

Unfortunately, although there is broad agreement on many elements of energy loss calculations, different numerical results may vary widely. However, despite the uncertainty, simple kinematic arguments give significant information about the dependence on  $L$  and density.

## 4 Conclusions

High-energy electrodynamic reactions are highly sensitive to their environment. In-medium effects can drastically change the cross sections of bremsstrahlung and pair production. Individual target atoms are indistinguishable, and the electron or photon projectiles interact with the medium as a whole. At the highest energies, it becomes impossible to separate electromagnetic showers into individual reactions, and current theoretical approaches break down.

Similar effects occur for hadronic reactions in dense media such as heavy ions. In some cases, kinematics-derived scaling laws can explain the in-medium effects, while in others, more work is needed.

## Acknowledgments

The author would like to thank Bill Marciano and Sebastian White for organizing an enjoyable conference. This work was supported by the U.S. D.O.E. under contract DE-AC03-76SF00098.

## References

1. H. A. Bethe and W. Heitler, Proc. R. Soc. London, Ser. A **146**, 83 (1934)
2. E. L. Feinberg, Priroda Vol 1, pg. 30 (1994).
3. L. D. Landau and I. J. Pomeranchuk, Dokl. Akad. Nauk SSSR **92**, 535 (1953); L. D. Landau and I. J. Pomeranchuk, Dokl. Akad. Nauk SSSR **92**, 735 (1953).
4. M. L. Ter-Mikaelian, *High Energy Electromagnetic Processes in Condensed Media*, John Wiley, New York, 1972.
5. S. Klein, Rev. Mod. Phys. **71**, 1501 (1999).
6. A. B. Migdal, Phys. Rev. **103**, 1811 (1956).
7. V. N. Baier and V. M. Katkov, Phys. Rev. **D57**, 3146 (1998).
8. V. M. Galitsky and I. I. Gurevitch, Nuovo Cim. **32**, 396 (1964).
9. N. F. Shul'ga and S. P. Fomin, JETP Lett. **63**, 837 (1996).
10. A. Varfolomeev *et al.*, Sov. Phys. JETP **42**, 218 (1976).
11. K. Kasahara, Phys. Rev. **D31**, 2377 (1985).
12. P. Anthony *et al.*, Phys. Rev. Lett. **75**, 1949 (1995); P. Anthony *et al.*, Phys. Rev. **D56**, 1373 (1997).
13. P. Anthony *et al.*, Phys. Rev. Lett. **76**, 3550 (1996).
14. T. H. Bauer, R. D. Spital, D. R. Yennie and F. M. Pipkin, Rev. Mod. Phys. **50**, 261 (1978).
15. S. Klein, hep-ph/9808235, in *Proc. IVth Wkshp. on Quantum Chromodynamics*, June 1-6, 1998, Paris, France, ed. H. M. Fried and B. Müller, World Scientific, 1999.
16. R. Baier, D. Schiff and B. G. Zakharov, Ann Rev. Nucl. Parti. Sci. **50**, 37 (2000).